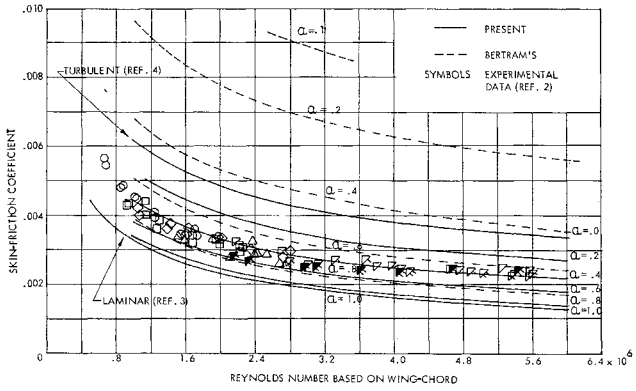

Fig. 2 Skin-friction coefficient of a delta wing with boundary-layer transition at $M_\infty = 6.8$.

where $R(x_T)$ is the Reynolds number based on the downstream distance from the actual leading edge to the transition line. The basic problem is that of determining the location of the transition line. Although analytical methods are not available for predicting the transition line at supersonic Mach numbers, empirical formulas such as that available in Ref. 5 may be used. If such empirical formulas are not applicable, then the transition line should be determined by direct experimental measurements.

The total skin-friction drag coefficient can be evaluated in terms of the coefficients for the two regions defined in Fig. 1 as follows: 1) the mixed flow region defined by the area *AFGED* and 2) the pure laminar regions defined by the areas *DEB* and *FCG*.

As a direct consequence of Eq. (1), the skin-friction coefficient formulas for turbulent flow [Eq. (3)] can be used in the first region, provided the Reynolds number is based on the distance measured from the virtual leading edge to the trailing edge of the delta wing. For the laminar region, Eq. (2) should be used. The expression for the total skin-friction drag coefficient based on the wing area can be written as follows:

$$C_F = \frac{4}{bc}\left\{\int_0^{b/c x_T} C_f(x)x\,dy + \int_{bc/x_T}^{b} C_f(\bar{x})\bar{x}\,dy\right\} \quad (5)$$

where $x = (c/b)y$ and $\bar{x} = (c/b)y + (\bar{x}_T - x_T)$.

Equation (5) can be written in dimensionless form by using the wing-chord as a reference length. Let

$$\xi = x/c \qquad \bar{\xi} = \bar{x}/c \quad (6)$$

and express the transition distance x_T as a percentage of the wing-chord,

$$a = x_T/c \quad (7)$$

Equation (5) becomes

$$C_F = 4\left\{\int_0^a C_f(c\xi)\xi\,d\xi + \int_a^1 \bar{C}_f(c\bar{\xi})\bar{\xi}\,d\bar{\xi}\right\} \quad (8)$$

where

$$\bar{\xi} = \xi + \{[R(x_T)/R(c)] - a\} \quad (9)$$

Equation (8) can be integrated in closed form by using Eq. (9) and the expressions for C_f and $\bar{C}_f$ given, respectively, by Eqs. (2) and (3). This result is provided as follows:

$$C_F = 4\left\{\frac{2A}{3R(c)^{1/2}}a^{3/2} + \frac{qD}{(2q-1)R(c)^{1/q}} \times \left[\left(1 + \frac{R(\bar{x}_T)}{R(c)} - a\right)^{(2q-1)/q} - \left(\frac{R(\bar{x}_T)}{R(c)}\right)^{(2q-1)/q}\right]\right\} \quad (10)$$

wherein the expression for $R(\bar{x}_T)/R(c)$ can also be written in terms of the parameter a as follows:

$$\frac{R(\bar{x}_T)}{R(c)} = \frac{[(A/D)a^{1/2}R(c)^{1/2}]^{q/(q-1)}}{R(c)} \quad (11)$$

Based on Eqs. (10) and (11), the skin-friction coefficient at a given Mach number can be determined as a function of Reynolds number once the location of the transition as a fraction of wing-chord a is known. For the purposes of comparison with Bertram's results,[2] Eq. (10) was evaluated at $M = 6.8$ wherein values of A, D, and q (given in Ref. 2) were used, i.e., $A = 1.22$, $D = 0.243$, and $q = 3.03$. These results are plotted in Fig. 2 as a function of the Reynolds number based on wing-chord, and the transition parameter a. Also shown are Bertram's results together with the experimental data that was also available in Ref. 2, Fig. 15. Comparison of Fig. 2 indicates that although the results for the laminar case, $a = 1.0$, agree with Bertram, the results for the turbulent region, $a = 0$, do not agree. The turbulent skin-friction drag based on the present paper does agree, however, with the results given by Van Driest.[4] Consequently, when the experimental data is compared with the theoretical curves for various values of a in Fig. 2, the interpretation of the data with respect to the amount of turbulent and laminar flow that exists is subject to question. For example, if the experimental data is compared with Bertram's curves in Fig. 2, the value of a would be from $a = 0.65$ to 0.75 which indicates that the flow on the wing is primarily laminar. On the other hand, if curves of the present paper are used, values of $a = 0.35$ to 0.45 are obtained which indicate that the flow on the wing is primarily turbulent.

References

[1] Schlichting, H., *Boundary Layer Theory* (McGraw-Hill Book Company Inc., New York, 1955), 3rd ed., Chap. XXI, p. 541.

[2] Bertram, M. H., "Boundary-layer displacement effects in air at Mach numbers of 6.8 and 9.6," NASA TR R-22 (1959).

[3] Bertram, M. H., "An approximate method for determining the displacement effects and viscous drag of laminar boundary layers in two-dimensional hypersonic flow," NACA TN 2773 (1952).

[4] Van Driest, E. R., "Turbulent boundary layer in compressible fluids," J. Aeronaut. Sci. **18**, 145–160 (1951).

[5] Deem, R. E., Erickson, C. R., and Murphy, J. S., "Flat-plate-boundary-layer transition at hypersonic speeds," Flight Dynamics Lab. TDR-64-129 (1964).

A 20-Ft-Diam Ribbon Parachute for Deployment at Dynamic Pressures above 400 PSF

WILLIAM B. PEPPER*
Sandia Laboratory, Albuquerque, N. M.

Introduction

IN order to satisfy the continual need for recovery systems capable of deployment at higher dynamic pressures, a parachute research program has been carried on over the last ten years to increase the capability of ribbon parachutes from

Received January 26, 1967. This work was supported by the U. S. Atomic Energy Commission. [10.09]

* Parachute Project Leader, Rocket and Recovery Systems Division, Aero- and Thermodynamics Department. Associate Fellow AIAA.

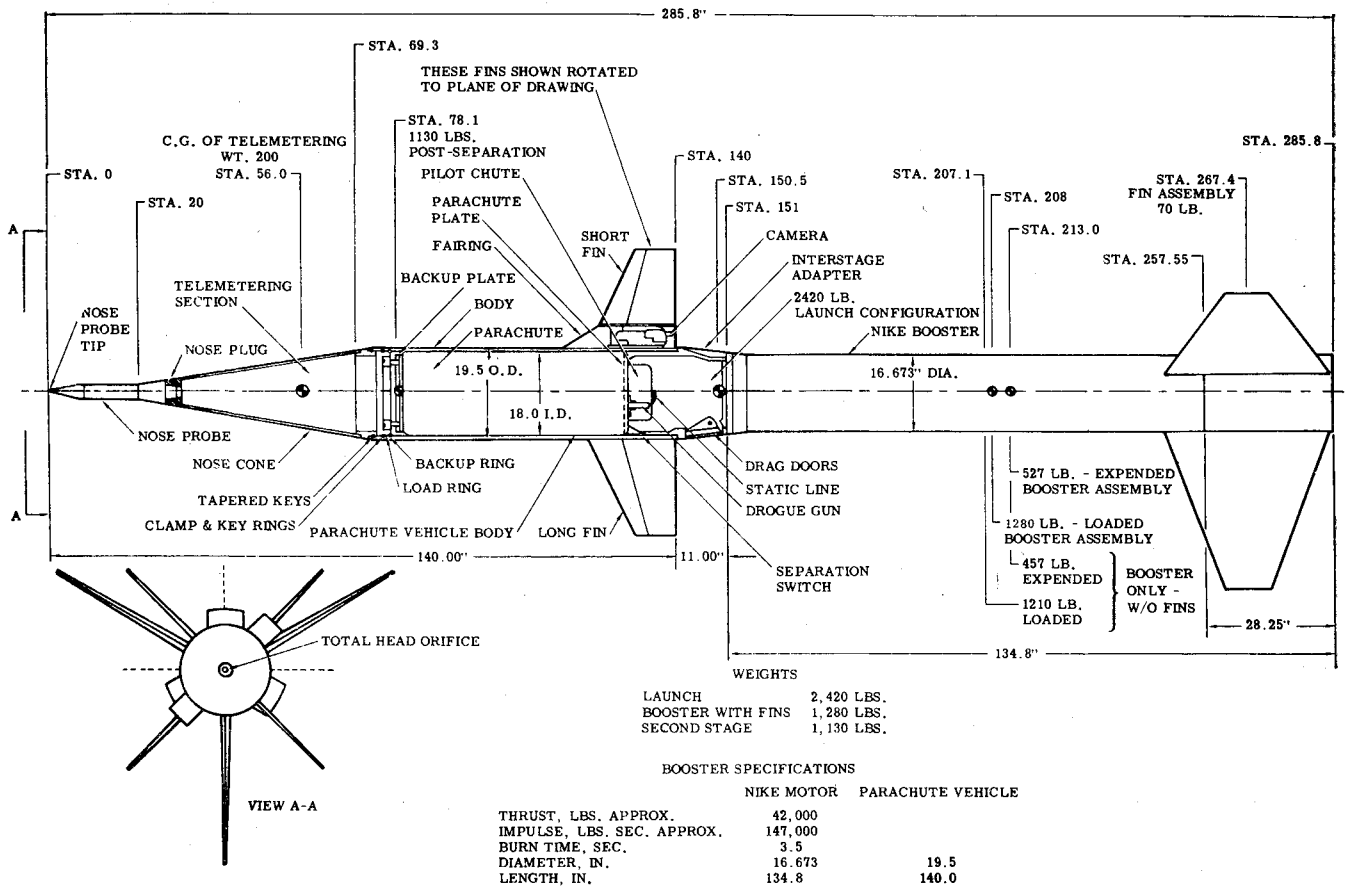

Fig. 1 SPTV assembly.

subsonic up to Mach 3.0. The parachute used for these tests was a specially designed 20-ft-diam chute developed by Sandia Corporation using a new type of reinforced selvage ribbon and specially designed 12,000-lb tensile strength suspension lines.

Apparatus

The parachute test vehicle shown in Fig. 1 is 19.5 in. in diameter and 12 ft long with a cone-spike nose for impact attenuation. An 8-channel telemetering system in the vehicle is used to measure deceleration of the unit after parachute deployment. The parachute is deployed at the desired dynamic pressure by a preset pressure switch that measures total head pressure at the center of the spike flat face. The vehicle is rocket boosted from a zero length launcher, shown in Fig. 2, by two Nikes firing in sequence. An electronic timer is used to fire the second Nike, start two photosonic onboard cameras, and to provide a backup parachute deployment signal. A 1-lb slug drogue gun is fired by a gas generator cartridge to deploy a heavy duty 18-in.-diam guide surface pilot chute that deploys the bag containing the 20-ft-diam ribbon parachute. The 30-gore, 20-deg conical ribbon chute was constructed of special 2000-, 3000-, and 4000-lb tensile strength reinforced selvage ribbon shown in Fig. 3. The increased edge material of this new ribbon design provides for better structural efficiency in tension and greater resistance to failure caused by tearing, which can produce complete gore failure with standard flat ribbon if one ribbon fails. The parachute system weighs approximately 180 lb.

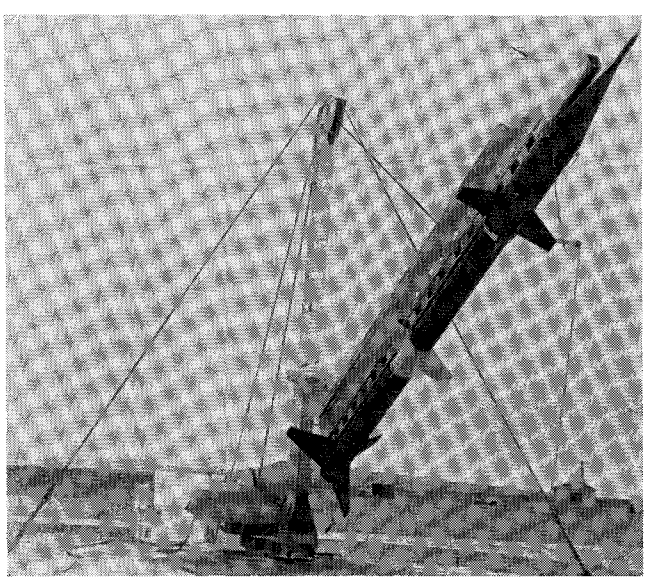

Fig. 2 RFTV high Mach number parachute test vehicle boosted by two Nikes.

Results

Parachute performance data[1] have been obtained on nine tests with the 20-ft-diam ribbon chute being deployed at dynamic pressures between 1710 and 4290 psf corresponding to Mach numbers of 1.39 to 2.21. The maximum deceleration at parachute opening is shown in Fig. 4 as a function of the deployment dynamic pressure. The highest load recorded was 130 g's, which would be a load of 143,000 lb on the vehicle. A 14-ft-long reefing line was used at the higher speeds to limit the maximum load on the chute. The first-stage average filling time was 0.1 sec. A 2-sec reefing delay was used with the Sandia Corporation "Half-Moon" pyrotechnic cutter. Some canopy oscillation or sidewise flapping was noted at the highest test Mach number, but the retardation performance

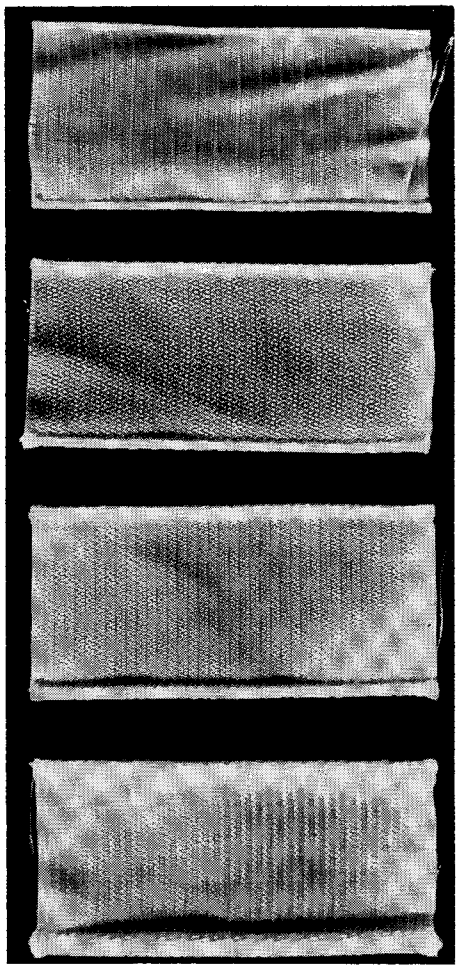

Fig. 3 Reinforced selvage ribbon—from top to bottom are shown 1000-, 2000-, 3000-, and 4000-lb tensile strength.

was adequate to slow the vehicle down rapidly; and disreefing allowed the chute to go full open so the impact velocity would be low enough to allow the nose-spike to penetrate the ground and leave the vehicle standing upright, as shown in Fig. 5.

Conclusions

A series of nine Nike rocket-boosted parachute tests have been conducted from which the following conclusions can be drawn: 1) The specially designed 20-ft-diam ribbon parachute can be used to recover a 1100-lb payload up to a Mach number of 2.2 and a dynamic pressure of 4300 psf. 2) The new reinforced selvage ribbon has been instrumental in perfecting parachutes that will operate in the environment previously described.

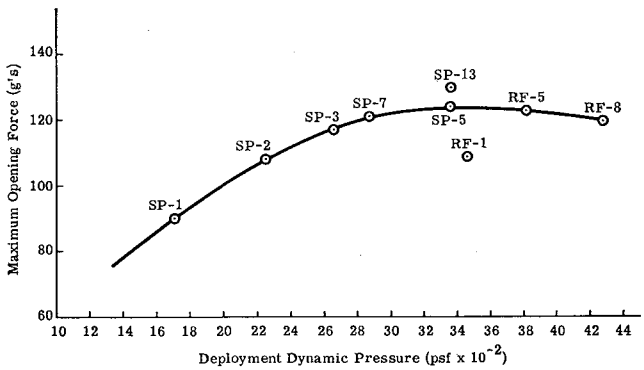

Fig. 4 Variation of maximum opening force with dynamic pressure.

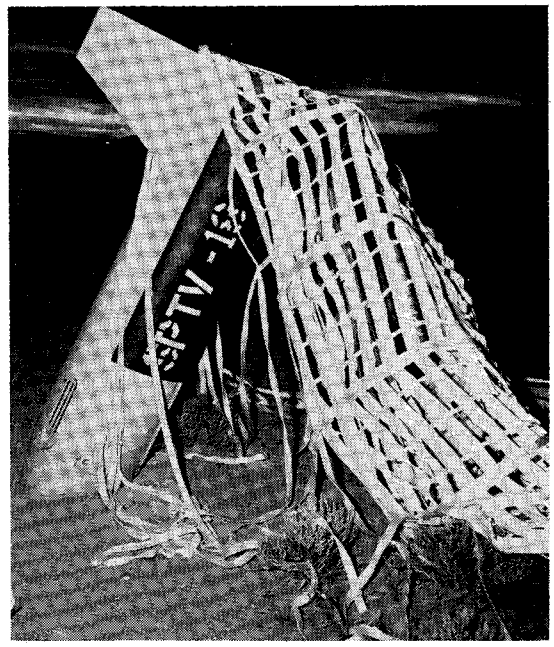

Fig. 5 Vehicle and 20-ft-diam parachute after successful test at Tonopah Test Range, Nev.

Reference

[1] Kane, M. T., "Design and testing of a 20-foot-diameter ribbon parachute for deployment at high dynamic pressures," Sandia Corp., SC-RR-66-79 (April 1966).

Determination of Subsonic Drag Rise by Hodograph Plane Analysis

M. S. Cahn* and G. M. Andrew†
Northrop Norair, Hawthorne, Calif.

Introduction

Previous work by Piercey[1] has shown that the drag divergence Mach number for an airfoil can be determined by studying the conditions at the crestline of the section. However, the physical significance of the crestline rule of thumb remains vague. The importance of the crestline was discovered by British workers from examination of plots of pressure coefficient vs Z (vertical distance) rather than the usual presentation of pressure coefficient vs percent chord.

It now seems that a hodograph representation may give a better understanding of the conditions for the formation of a strong shock or drag divergence. It can be shown that the conditions for the existence of flow breakdown can be determined from the hodograph plane. Where a decelerating streamline becomes tangent to the characteristic lines in the hodograph plane, steady isentropic flow will break down and a limit line will exist.

A study of this hodograph analysis suggested a direct method for transonic airfoil design. These concepts seem able to explain the physics of the crestline rule. Also indicated is the possibility of using large trailing edge angles with boundary-layer control to prevent separation.

Submitted December 28, 1966; also presented as Paper 67-4 at the AIAA 5th Aerospace Sciences Meeting, New York, January 23–26, 1967. [3.02]

* Research Aerodynamicist. Member AIAA.
† Research Aerodynamicist. Associate Fellow AIAA.